AB

TRI-PP-91-47
May 1991

Pion Induced Pion Production on Deuterium and Hydrogen

V. Sossi, M.J. Iqbal, R.R. Johnson, G. Jones, M. Pavan, F.M. Rozon*, M. Sevior, D. Vetterli, P. Weber†
Department of Physics, University of British Columbia, Vancouver, B.C., Canada V6T 1Z1
G. Sheffer, G.R. Smith
TRIUMF, Vancouver, B.C., Canada V6T 2A3
P. Camerini, N. Grion, R. Rui,
Dipartimento di Fisica dell'Università di Trieste, 34127 Trieste, Italy and Istituto Nazionale di Fisica Nucleare, 34127 Trieste, Italy
N.R. Stevenson
Department of Physics, University of Saskatchewan, Saskatoon, Sask., Canada S7N 0W0
M.J. Vicente-Vacas
Departamento de Física Teórica and IFIC, Centro mixto Universidad de Valencia CSIC, E-46100, Valencia, Spain

Abstract

A detailed experimental analysis of the $\pi^+ d \rightarrow \pi^+\pi^- pp$ in-plane coincidence data first presented by Rui et al.[1] is used to test an expanded version of the Oset and Vicente-Vacas model[2] for pion induced pion production on a free nucleon. This extended model includes nine additional diagrams to account for the $N^* \rightarrow N(\pi\pi)_{p-wave}$ reaction channels and averages over Fermi motion to describe the quasifree nature of the process occurring on the deuteron. Experimental effects such as pion energy loss in the target and in the detectors, pion decay and muon detection are investigated and incorporated into the comparison of experimental data and theory. Very good overall agreement between data and theory is achieved without requiring a significant contribution from four body reaction mechanisms. When compared to the total cross section measurements of Manley et al.[3], the model yields a model dependent determination of the overall strength of the diagram containing the $N^* \rightarrow N(\pi\pi)_{s-wave}$ vertex. The sensitivity of the cross section to the variation of the $\Delta\pi\Delta$ (f_Δ) and $N^*\Delta\pi$ ($g_{N^*\Delta\pi}$) coupling constants is also studied.

(submitted to Physical Review C)

*Present address: Physics Department, Carnegie Mellon University, Pittsburgh PA, USA 15213
†Present affiliation: IMP/ETH, mailing address: EP-Div CERN, 1211 Geneve 23, Switzerland

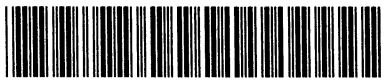

TRI-PP 91-47
fw9136

1. Introduction

Pion induced pion production is the dominant πN strong inelastic channel for pion energies below 1 GeV and above the pion production threshold. This feature, together with the fact that the reaction also involves a $\pi\pi$ interaction vertex and a high isospin selectivity through the selection of the initial and final pion charge states makes it a very attractive choice for experimental and theoretical work. Isospin conservation limits the number of allowed intermediate states for each reaction channel thus providing a relatively simple and selective environment for the possible determination of the reaction mechanisms and of the constants. The determination of the $\Delta\pi\Delta$ (f_Δ) coupling constant is of particular interest since this vertex also contributes to the Double Charge eXchange (DCX) reaction through the Delta-nucleon INTeraction mechanism (DINT)[4]. By its very nature the DCX reaction involves two nucleons and can be used to study nucleon-nucleon correlation functions once the reaction mechanism is thoroughly understood. At present there are no direct measurements of the f_Δ coupling constant. The existing theoretical predictions tend to agree on values close to 1.0 (expressed in units of $4/5\ f_{NN\pi}$)[5-9], while the analysis of several isospin channels of the free pion induced pion production reaction by Arndt et al.[10] shows a preference for values around 0.4.

The other relevant feature of the pion induced pion production reaction is that the $\pi\pi$ interaction vertex is related to the isospin zero and isospin two $\pi\pi$ s-wave scattering lengths a_0^0 and a_2^0. A very accurate measurement of these quantities would permit the determination of the coefficient of the fourth order term in the momentum expansion of the quark Lagrangian in chiral perturbation theory. Such a result would discriminate amongst different theoretical approaches[12,13]. A clear understanding of the reaction mechanism is thus important.

Theoretical efforts to describe the free pion induced pion production reactions can be roughly divided into two main streams. Both use effective Lagrangians derived from current algebra to describe that part of the reaction mechanism which involves only pions and nucleons, while the intermediate isobar states are described either with an isobar model partial-wave analysis[10,3] or via Feynman diagrams[2,14]. The model presented in this paper is based on the second approach. We have taken existing total cross section data[3] as well as a detailed analysis of the π^+d $\rightarrow \pi^+\pi^-$p p data first presented in ref.[1] and compared them with an extended version of the Oset and Vicente-Vacas model first given in ref.[2]. This paper describes briefly the deuterium experiment itself, but focusses primarily on the description of the corrections that were made in order to compare the experimental spectra with theoretical calculations, the extension of the theoretical model, and the inclusion of Fermi motion to make the model applicable to deuterium.

2. Experiment and Data Analysis

The π^+d $\rightarrow \pi^+\pi^-$p p experiment performed at TRIUMF at an incident beam energy of 280 MeV has been reported in refs.[1,15,16]. The following is a brief summary of the experimental details.

We chose a deuterium target (π^+d $\rightarrow \pi^+\pi^-$p p) as opposed to a hydrogen target (π^-p $\rightarrow \pi^+\pi^-$n) for the study of the free process to be able to take advantage

of the more intense TRIUMF π^+ beam[17]. This choice was justified by earlier experimental resultsitekn:lich that demonstrated that the pion induced pion production on deuterium was consistent with a quasifree process on a single nucleon.

The positive and negative outgoing particles were detected with an in-plane coincidence apparatus which also provided information concerning the particle energies as well as their polar angles. Negative pions were identified by a quadrupole-quadrupole-dipole (QQD) spectrometer[19], while positive pions were selected by the total absorption range telescope CARUZ[20]. The apparatus settings are listed in table 1.

The four-fold differential cross sections:

$$\frac{d^4\sigma}{dT_{\pi^+}\,dT_{\pi^-}\,d\Omega_{\pi^+}\,d\Omega_{\pi^-}}$$

were extracted from the data, after correcting for the response of the detectors over the allowed range of pion energies and angles and in part for pion decay as described below. The finite size of the target was also taken into account.

The corrections for π^- detection on the QQD side were straightforward. This spectrometer is capable of rejecting electrons and muons so that an unambiguous π^- spectrum could be obtained. When the coincidence events were binned to establish cross sections, a weighting factor accounting for the fraction of the pions that decayed while traversing the apparatus was applied on an event by event basis[21]. Similarly the solid angle for each event was normalized to the nominal QQD solid angle (18 msr) with an additional weighting factor rendering the spectrometer angular acceptance independent of the pion momentum. These corrections have been used in a previous experiment[21]. The lowest π^- energy limit of the data used in the analysis presented in this paper was 30 MeV. Above this energy the effects of multiple scattering and of the finite target size were found to be negligible. Consequently no correction was necessary for these effects.

Multiple scattering effects could also be neglected on the side of the CARUZ detector, since the mean value of the multiple scattering angle was within the angular resolution of the detector. Likewise the effects of hadronic interaction were found to be negligible. On the other hand, the CARUZ could not discriminate between pions and those muons resulting from pion decay between the production point and the end point of the CARUZ. Only a fraction of these muons was detected and they were, of course, recorded with a different angle and energy from those of the original pions. The scintillator elements were too thick to give a range energy separation between pions and muons. Consequently, this effect introduced a source of distortion in the yield and shape of the four-fold differential cross section as a function of the kinetic energy of the positive pions (T_{π^+} spectra). Another source of such distortion was the finite size of the target, since both the detected energy of each pion and the detection efficiency for pions produced with less energy than necessary to traverse the target (12 MeV), depended on the location of the production point within the target. The pion loss due to the finite size of the target was relevant on the CARUZ side, since the low energy detection threshold of this instrument was 8 MeV for pions. Such a low energy threshold was desired to cover regions of phase space close to the lower kinematic limits of the reaction. Since this was a coincidence experiment the overall normalization of the negative pion distributions was however corrected to take into account the detection inefficiency of the CARUZ detector. This correction factor,

on average, enhanced the data by 25% and is included in the T_{π^-} and θ_{π^+} spectra shown here (where θ is the polar angle with respect to the beam direction) .

The T_{π^+} spectra presented in this paper are shown without corrections for pion decay and energy distortion. Instead these effects were convoluted with the T_{π^+} theoretical spectra when comparing theory to experiment. This was achieved by computer simulation of the experimental conditions using Monte Carlo techniques[16]. Theoretical spectra describing the pion energy distribution at their production point and constrained by the experimental energy and angular detection windows were used as input to the program. The program, operating on an event by event basis, selected randomly the pion production coordinate along the beam direction within the physical dimensions of the target, while the two transverse coordinates were selected according to a gaussian distribution in order to simulate the beam profile. The pion decay probability was then calculated as a function of position along the pion trajectory from its production point in the cylindrical deuterium target to the CARUZ scintillators. If a Monte Carlo pion decayed along its trajectory, then the energy and trajectory of the resultant muon were obtained from the $\pi \rightarrow \mu$ decay energy and angular distributions. The software veto imposed by a signal from the last scintillator of the CARUZ stack used during the data analysis to guarantee that the particle stopped in the detector was also incorporated as a veto in the Monte Carlo program. For each input spectrum the program generated an output spectrum describing the measured kinetic energy of the particles detected by the CARUZ. This spectrum is compared to the data in fig. 5,6 and 8. Note that the spectral distortion due to the experimental conditions yields events outside the pure three body phase space.

The inverse of the ratio between the yield of output spectrum of the program and the input spectrum provided the multiplicative correction factor for the yields of the T_{π^-} and θ_{π^+} spectra mentioned earlier. The shapes of these last two spectra were found not to be significantly affected by the distortion of the shape of the T_{π^+} spectra, since negative pions from the same energy bin have the corresponding π^+'s spread over a range of energy wide enough to allow for an average correction factor. Likewise the positive pions in the same angular bin have a fairly uniform energy distribution when averaged over all T_{π^-}.

3. Theoretical Model

The interpretation of the experimental results is based on an extended version of the Oset and Vicente-Vacas Monte Carlo model[2] that describes the free pion induced pion production process: $\pi^-\mathrm{p} \rightarrow \pi^+\pi^-\mathrm{n}$. They describe the reaction mechanism with Feynman diagrams involving nucleons, Δ's and Ropers in the intermediate state. Only that fraction of the N^* (1/2,1/2) Roper resonance that decays into two pions in a relative S state is included in their model. There are three parameters in their model that are not well determined: the chiral symmetry breaking parameter, ξ, which arises from the part of the model derived from the Weinberg Lagrangians, the $\Delta\pi\Delta$ coupling constant and the overall strength of the diagrams containing the the $N^* \rightarrow N(\pi\pi)_{s-wave}$ vertex (fig. 2.d). This last parameter is a product of the $N^* \rightarrow N(\pi\pi)_{s-wave}$ coupling constant, C, and the $N^*N\pi$ coupling constant $g_{N^*N\pi}$[23], both uncertain by about 100%. In the present model we fixed ξ to be zero, which is

consistent with soft pion theory[24-26] and the value of the $N^*N\pi$ coupling constant to 0.02, which is the value used in ref.[2] ($g_{N^*N\pi}$range 0.01 to 0.02).

3.1. New Diagrams

As the Oset and Vicente-Vacas model[2] underestimates the total cross section measurement at our energies by about 50%[3,27], additional intermediate state contributions were examined. A contribution that was missing in ref.[2] arises from diagrams that describe the $N^* \rightarrow N(\pi\pi)_{p-wave}$ decay fraction. We considered the diagrams listed in fig. 1. The first four containing a ρ meson were neglected. At $T_\pi = 280$ MeV the invariant mass of the two pions is small compared to the ρ mass, thus supressing the contribution of these diagrams. The contribution of diagram 1.c) was also neglected, since in this case a real pion is emitted before the formation of the N^*. This leaves the system with an energy (1160 MeV) which is too far from the N^* resonance peak to favour its formation. For the same reason only the first nucleon propagator in 1.b) was replaced by the N^* propagator. All diagrams now included in the model are shown in fig.2 and the amplitudes related to the new diagrams are presented in Appendix A.

In addition to the coupling constants used in[2] the new set of diagrams required the $N^*\Delta\pi$ coupling constant. The allowed values of this coupling constant were calculated from the $N^* \rightarrow N(\pi\pi)_{p-wave}$ decay branching ratio[28] and they ranged between 1.1 m_π^{-1} and 1.5 m_π^{-1}. The contribution of the new diagrams to the total cross section at $T_{\pi^+} = 280$ MeV with $g_{N^*\Delta\pi} = 1.3\ m_\pi^{-1}$ (an intermediate value of this coupling constant) and $g_{N^*N\pi} = 0.02$ is about 15%.

The C coupling constant has also been recalculated from the $N^* \rightarrow N(\pi\pi)_{s-wave}$ decay branching ratio. The present limits are -3.0 m_π^{-1} and -1.5 m_π^{-1} in contrast with the -1.11 m_π^{-1} to -0.71 m_π^{-1} range quoted in the earlier Oset and Vicente-Vacas calculations. With the recalculated range of values of C the model overlaps the experimental results in the energy range from reaction threshold to 280 MeV[29,3].

4. Cross section sensitivity to coupling constant variation and determination of C

We first explored the sensitivity of the theoretical cross section to the parameter variation in the energy range from reaction threshold to 280 MeV. We considered 280 MeV to be the upper energy limit for the applicability of the model, since at higher energies the contribution of other resonances becomes significant. The cross section was calculated for the quoted lower and upper limit of the C and $g_{N^*\Delta\pi}$ coupling constants separately, maintaining the other parameters at a fixed value. We arbitrarily set f_Δ to be 0.5 and 1.0 to explore the cross section sensitivity to the variation of this parameter. The results are presented in table 2. Throughout this energy range the cross section is clearly most sensitive to the variation of the C parameter reflecting the very significant contribution of the $N^* \rightarrow N(\pi\pi)_{s-wave}$ diagrams. The importance of these diagrams is also noticeable in fig.3 where the three curves compare the total cross section calculated with the pion pole term only, with the pion pole term plus these N^* diagrams and the full calculation. The total cross section shows some sensitivity to the variation f_Δ and $g_{N^*\Delta\pi}$ only at energies

above 250 MeV. On the basis of these results we determined C by fitting the energy dependence of the model to the four total cross section measurements of ref.[3] (203, 230, 255 and 280 MeV), while we used our differential cross section data at 280 MeV for a more detailed test of the model. With $\xi = 0.0$, $g_{N^*\Delta\pi} = 1.5\ m_\pi^{-1}$ and $f_\Delta = 1.0$ we determined the product of C and $g_{N^*N\pi}$ to be -$(4.14 \pm 0.08)\times10^{-2} m_\pi^{-1}$ using the standard χ^2 technique. Consequently, taking $g_{N^*N\pi}$ to be 0.02 as in ref.[2], C falls in the range -2.07±0.04 m_π^{-1}. This range of values of C determines the $N^* \rightarrow N(\pi\pi)_{s-wave}$ decay branching ratio to be about 10%, consistent with the published values[28]. Fig. 4 shows the theoretical cross section as a function of energy with C fixed to -2.08m_π^{-1} compared to the experimental values. The value C = -2.08 m_π^{-1} was selected for the analysis described in the next sections.

5. Comparison to the four-fold differential cross section data and to Other Data

With C determined from total cross section data we examined the differential cross section data of our experiment. The calculations that have been presented to this point are free process calculations. To compare them to our experiment on the deuteron the addition of the Fermi motion to the model was required.

5.1. Fermi Motion

The Fermi motion was taken into account by introducing an initial momentum for the nucleon into the Monte Carlo program describing the free process. The nucleon was treated as an off-shell particle with its energy equal to its mass and its momentum randomly chosen according to the Hulthen nucleon momentum distribution[30]. The procedure is described in detail in ref.[16].

The effect of the Fermi motion is to broaden and to smear the kinematic ranges allowed for the outgoing particles. This effect becomes particularly evident in the kinematic region close to the free reaction phase space limits. Two such regions fall in the range of our detectors and in both cases the effect of Fermi motion is significant as shown in fig. 5 (the two theoretical curves are calculated with the same set of parameters C=-2.08 m_π^{-1}, $g_{N^*\Delta\pi}$=1.5 m_π^{-1} and f_Δ=1.0). In ref.[1] data in these regions were observed to depart from the predictions of the model of[2]. However nucleon Fermi motion was not included in the previous comparison.

Even in the present analysis there is still a difference between the limits of the theoretical cross sections and the data in fig. 5 (upper two fig.) and fig. 6 in the high energy region. However this difference did not affect the quantitative comparison of the data with theory.

5.2. Determination of f_Δ and $g_{N^*\Delta\pi}$.

After fixing the C value to -2.08 m_π^{-1}, introducing Fermi motion and applying the necessary experimental corrections, the theoretical T_{π^+}, θ_{π^+} and T_{π^-} distributions were calculated using 15 different sets of parameters. We compared them to data using the χ^2 technique. We varied $g_{N^*\Delta\pi}$ from its lower to its upper limit with one intermediate step at $g_{N^*\Delta\pi} = 1.3\ m_\pi^{-1}$ and for each of them we tested five different values of f_Δ: 0.0, 0.1, 0.5, 1.0 and 2.0. This last value was chosen to confirm the validity of the accepted range of values. In fig. 6-9 we compare the theoretical

distribution obtained with sample parameter sets to the experimental spectra. As an overall feature the curves associated with the values of f_Δ equal to or smaller than 1.0 agree with the data well, while the curves associated with the value f_Δ=2.0 overestimate the data in almost all the spectra. A quantitative comparison was performed by calculating the reduced χ^2 averaged over the T_{π^+}, θ_{π^+} and T_{π^-} distributions. The results are summarized in fig. 10 which shows the reduced χ^2 values as a function of the different values of the coupling constants. The curves indicate that a clear minimum value of the χ^2 distribution cannot be found for any particular value of the coupling constants, but with this model we can definitely rule out f_Δ values larger than 1.0 for any value of $g_{N^*\Delta\pi}$. The smallest value of $g_{N^*\Delta\pi}$ seems to be favoured except for f_Δ values very close to zero, where there are no preferred $g_{N^*\Delta\pi}$ values.

5.3. Comparison to Other Data

Since there is no strongly preferred set of coupling constants we could not rigorously determine the coupling constant values. We could still achieve a model dependent estimate of the total cross section from our experimental data by calculating its value for a number of sets of parameters that provided agreement between the model differential cross sections and our data. Using these parameters we then calculated the total cross section for the quasifree process ($\pi d \rightarrow \pi\pi NN$) at T_π = 256 MeV and for the free process ($\pi^- p \rightarrow \pi^+\pi^- n$) at T_π = 280 MeV. The quasifree calculation at T_π = 256 MeV agreed with the measurement of Lichtenstadt et al.[18] in all cases, while the calculation for the free process at T_π = 280 MeV underestimated the experimental value by more than two standard deviations even with those values of the coupling constants that provided the highest cross section value (see table 3).

6. Discussion

There are some important observations arising from the comparisons described in the previous paragraph. The model fits the experimental total cross sections up to about T_π=250 MeV but underestimates it by about 15% at T_π=280 MeV. The model does however reproduce differential cross section data at T_π=280 MeV. Therefore the model may lack mechanisms that contribute to the total cross section at higher energy in a region of phase space not covered by our experiment. Possible contributions of this type could arise from heavier N^* isobars in the intermediate state.

Since the various diagrams in the theory contribute differently to the cross section in different isospin channels, a further test of the model could be provided by a more comprehensive experiment that would measure pion induced pion production in a variety of charge states. Such an extended experiment would also facilitate determination of the coupling constants, since different isospin channels provide different constraints. For example a larger f_Δ value decreases the $\pi^+ p \rightarrow \pi^+\pi^+ n$ cross section, while it increases the $\pi^- p \rightarrow \pi^+\pi^- n$ cross section.

A similar comparison between experiment and theory was performed by Ortner et al.[31], where a somewhat different model was employed[14]. They do not account for the ϵ induced contribution[32] and treat the off-shell pion in the pion-pole term differently. In a preliminary analysis they concluded that their model underestimates the in-plane reaction cross section in contradistinction with our results. However,

since the two theoretical models are different, the two conclusions are not necessarily contradictory.

7. Conclusion

We extended the existing[2] model to pion production on deuterium in the energy range of interest by incorporating additional diagrams and allowing for Fermi motion of the contributing nucleon. We demonstrated that the model reproduces the differential data at T_π = 280 MeV and the total cross section measurements up to about 250 MeV.

Within the framework of the model we determined the C parameter for the $N^* \rightarrow N(\pi\pi)_{s-wave}$ to be approximately -2.1 m_π^{-1} with ξ fixed to 0.0 and $g_{N^*N\pi}$ to 0.02. We demonstrated a preference of the $\Delta\pi\Delta$ coupling constant to be less than 1.0 in agreement with the analysis of Arndt et al.[10]. We did not detect significant sensitivity of the cross section to the $N^*\Delta\pi$ coupling constant in agreement with Ortner et al.[31]. However our data show a preference for the lower values within the estimated range.

These results contribute to the understanding of the overall mechanism of the free pion induced pion production reaction, even though we realize that they are not adequate to decouple the $N^*N\pi$ and C coupling constants nor to provide significantly improved limits on the coupling constants, $g_{N^*\Delta\pi}$ and f_Δ. A modification of the term describing the $\pi - \pi$ scattering amplitude in the model to include the pion rescattering should also be explored[12]. A more accurate description of this amplitude would certainly lead to a more precise and meaningful determination of the coupling constants, in particular C, since there is a strong correlation between the diagrams containing C and the pion pole term. We believe that a more stringent test of the model and consequently a more accurate determination of such parameters would result from comparing the theoretical distributions to a more extensive set of precise differential cross section measurements of the free process where there is no broadening of the angular and energy ranges due to Fermi motion. A natural candidate for further investigation is the reaction $\pi^+ p \rightarrow \pi^+\pi^+ n$. Due to isospin conservation constraints there are fewer intermediate states permitted in this reaction than in the $\pi^- p \rightarrow \pi^+\pi^- n$ case. It may thus be easier to isolate the contributions of each reaction mechanism. We are currently studying how the f_Δ coupling constant and the pion scattering length can be extracted from the measurement of the cross section of this reaction. Since the cross section for this process is about one order of magnitude smaller than that of $\pi^- p \rightarrow \pi^-\pi^+ n$ the energy and geometrical settings would have to be carefully planned in order to guarantee the maximum information from the data.

More extensive measurements of the in- and out- of the reaction plane cross section are needed for a more complete test of the model. A larger set of data would also allow a simultaneous parameter variation, making their determination more significant.

8. Aknowledgments

We express our thanks to Byron Jennings for all the useful and helpful discussions.

Appendix A
Amplitudes Related to the New Diagrams

In calculating these amplitudes we followed the convention of[2] for the Δ and N^* mass distribution. The N^* mass (M^*) is taken to be 1440 MeV and its width (Γ^*) at any energy is appropriately scaled to the width value at the peak energy (235$\pm$115 MeV[28]). The amplitudes related to the diagrams of fig. 1 are thus:

$$-iT^{3,N^*} = -(\tilde{f}/\mu)(f/\mu)^2 2\sqrt{2}\boldsymbol{\sigma}\cdot\boldsymbol{p}_5\boldsymbol{\sigma}\cdot\boldsymbol{p}_6\boldsymbol{\sigma}\cdot\boldsymbol{p}_1\times$$

$$\frac{i}{\sqrt{S}-p_6^0-m-\boldsymbol{p}_6^2/2m}\,\frac{i}{\sqrt{S}-M^*+(i/2)\Gamma^*}$$

$$-iT_a^{3,N^*} = -(\tilde{f}/\mu)(f^*/\mu)(g_{N^*\Delta\pi})\frac{\sqrt{2}}{3}\boldsymbol{\sigma}\cdot\boldsymbol{p}_5\;\boldsymbol{S}\cdot\boldsymbol{p}_6\;\boldsymbol{S}^+\cdot\boldsymbol{p}_1\times$$

$$\frac{i}{\sqrt{S}-m_\Delta+(i/2)\Gamma}\,\frac{i}{\sqrt{S}-p_6^0-\boldsymbol{p}_6^2/2M^*-M^*+(i/2)\Gamma^*}$$

$$-iT_b^{3,N^*} = -(\tilde{f}/\mu)(f^*/\mu)(g_{N^*\Delta\pi})\sqrt{2}\boldsymbol{S}\cdot\boldsymbol{p}_6\;\boldsymbol{S}^+\cdot\boldsymbol{p}_1\boldsymbol{\sigma}\cdot\boldsymbol{p}_5\times$$

$$\frac{1}{\boldsymbol{p}_1^2/2m+m-p_5^0-(\boldsymbol{p}_1+\boldsymbol{p}_5)^2/2M^*-M^*+(i/2)\Gamma^*}\,\frac{i}{\sqrt{S}-p_5^0-\boldsymbol{p}_5^2/2m_\Delta-m_\Delta+(i/2)\Gamma}$$

$$-iT_c^{3,N^*} = -(\tilde{f}/\mu)(f^*/\mu)(g_{N^*\Delta\pi})\sqrt{2}\boldsymbol{\sigma}\cdot\boldsymbol{p}_5\;\boldsymbol{S}\cdot\boldsymbol{p}_1\;\boldsymbol{S}^+\cdot\boldsymbol{p}_6\times$$

$$\frac{i}{\boldsymbol{p}_1^2/2m-p_6^0-\omega_R-(\boldsymbol{p}_1+\boldsymbol{p}_6)^2/2m_\Delta+(i/2)\Gamma}\,\frac{i}{\sqrt{S}-p_6^0-M^*+(i/2)\Gamma^*-\boldsymbol{p}_6^2/2M^*}$$

$$-iT_d^{3,N^*} = -(\tilde{f}/\mu)(f^*/\mu)(g_{N^*\Delta\pi})\frac{\sqrt{2}}{3}\boldsymbol{S}\cdot\boldsymbol{p}_1\;\boldsymbol{S}^+\cdot\boldsymbol{p}_6\boldsymbol{\sigma}\cdot\boldsymbol{p}_5\times$$

$$\frac{i}{\boldsymbol{p}_1^2/2m-p_5^0+m-M^*+(i/2)\Gamma^*-(\boldsymbol{p}_1+\boldsymbol{p}_5)^2/2M^*}\,\frac{i}{\boldsymbol{p}_1^2/2m-p_5^0-p_6^0-\omega_R-(\boldsymbol{p}_1+\boldsymbol{p}_5+\boldsymbol{p}_6)^2/2m_\Delta+(i/2)\Gamma}$$

$$-iT_e^{3,N^*} = -(\tilde{f}/\mu)(f^*/\mu)(g_{N^*\Delta\pi})\frac{\sqrt{2}}{3}\boldsymbol{\sigma}\cdot\boldsymbol{p}_1\;\boldsymbol{S}\cdot\boldsymbol{p}_6\;\boldsymbol{S}^+\cdot\boldsymbol{p}_5\times$$

$$\frac{i}{\boldsymbol{p}_1^2/2m-p_5^0-\omega_R-(\boldsymbol{p}_1+\boldsymbol{p}_5)^2/2m_\Delta+(i/2)\Gamma}\,\frac{i}{\boldsymbol{p}_1^2/2m-p_5^0-p_6^0+m-(\boldsymbol{p}_1+\boldsymbol{p}_5+\boldsymbol{p}_6)^2/2M^*+(i/2)\Gamma^*-M^*}$$

$$-iT_f^{3,N^*} = -(\tilde{f}/\mu)(f^*/\mu)(g_{N^*\Delta\pi})\sqrt{2}\boldsymbol{S}\cdot\boldsymbol{p}_6\;\boldsymbol{S}^+\cdot\boldsymbol{p}_5\boldsymbol{\sigma}\cdot\boldsymbol{p}_1\times$$

$$\frac{i}{\sqrt{s}-M^*+(i/2)\Gamma^*}\ \frac{i}{\sqrt{s}-p_5^0-m_\Delta-\vec{p}_5^{\,2}/2m_\Delta+(i/2)\Gamma}$$

$$-iT_g^{3,N^*} = -(\tilde{f}/\mu)(f^*/\mu)(g_{N^*\Delta\pi})\sqrt{2}\boldsymbol{\sigma}\cdot\boldsymbol{p}_1\ \boldsymbol{S}\cdot\boldsymbol{p}_5\ \boldsymbol{S}^+\cdot\boldsymbol{p}_6\times$$

$$\frac{i}{\vec{p}_1^{\,2}/2m-p_5^0-\omega_R-(\vec{p}_1+\vec{p}_6)^2/2m_\Delta+(i/2)\Gamma}\ \frac{i}{\vec{p}_1^{\,2}/2m-p_5^0-p_6^0+m-(\vec{p}_1+\vec{p}_5+\vec{p}_6)^2/2M^*+(i/2)\Gamma^*-M^*}$$

$$-iT_h^{3,N^*} = -(\tilde{f}/\mu)(f^*/\mu)(g_{N^*\Delta\pi})\tfrac{\sqrt{2}}{3}\boldsymbol{S}\cdot\boldsymbol{p}_5\ \boldsymbol{S}^+\cdot\boldsymbol{p}_6\boldsymbol{\sigma}\cdot\boldsymbol{p}_1\times$$

$$\frac{i}{\sqrt{s}-M^*+(i/2)\Gamma^*}\ \frac{i}{\sqrt{s}-p_6^0-m_\Delta-\vec{p}_6^{\,2}/2m_\Delta+(i/2)\Gamma}$$

where $\omega_R = m - m_\Delta$.

REFERENCES

1 R. Rui et al., Nucl. Phys. A517 (1990)455

2 E. Oset and M.J. Vicente-Vacas, Nucl. Phys. A446 (1985)584

3 D.M. Manley, Ph.D. Thesis, University of Wyoming, 1981 [Los Alamos National Lab. Report No. LA-9101-T, 1981]

4 M.B. Johnson et al., Phys. Rev. Lett. 52 (1984)593

5 Adler and Dashen Current Algebra and Application to Particle Physics, New York, W.A. Benjamin, 1968

6 G.E. Brown and W. Weise, Phys. Rep. 22 (1975)279

7 B. Sakita and K.C. Vali, Phys. Rev. 139B (1965)1355

8 D.G. Sutherland, Nuovo Cimento 48 (1967)188

9 R.P. Feynman et al., Phys. Rev. D3 (1971)2706

10 R.A. Arndt et al., Phys. Rev. D20 (1979)651

11 D.M. Manley, Phys. Rev. D30 (1984)536

12 J.Gasser and H.Leutwyler, Phys. Lett. 125B (1982)321 and 325

13 A.N. Ivanov and N.I. Troitskaya, Sov. J. Nucl. Phys. 43 (1986)260

14 G. Jäkel et al., Nucl.Phys. A511 (1990)733

15 R. Rui et al., The $(\pi, 2\pi)$ reaction on few body systems, Proceedings of the 12th International IUPAP Conference on Few Body Problems in Physics, Vancouver, Canada, July 1989

16 V. Sossi UBC PhD Thesis 1991 University of British Columbia, Vancouver, Canada unpublished

17 Triumf Users Handbook (1987)

18 J. Lichtenstadt et al., Phys. Rev. C33 (1986)655

19 R.J. Sobie et al., Nucl. Instr. and Methods 219 (1984)501

20 F.M. Rozon et al., Nucl. Instr. and Methods A267 (1988)101

21 N. Grion et al., Nucl. Phys. A492 1989(509)

22 F. James, FOWL, A General Monte Phase Space Program, 1977, CERN computer Centre Program Library

23 T. Ericson and W. Weise, Pions and Nuclei, p.29 Clarendon Press Oxford, 1988

24 S. Weinberg, Phys. Rev. Lett. 17, 616(1966)

25 S. Weinberg, Phys. Rev. Lett. 18, 188(1967)

26 M.G. Olsson and L. Turner Phys. Rev. Lett. 20, 1127(1968)

27 C.W. Bjork et al., Phys. Rev. Lett. 44 (1980)62

28 Phys. Lett. B239 (1990) Particle Properties Data Booklet, North Holland Amsterdam, 1988

29 M.E. Sevior et al., Phys. Rev. Lett. to be published

30 L. Hulthen and M. Sugakawa, Encyclopedia of Physics XXXIX (1957)1

31 H.W. Ortner et al., Phys. Rev. Lett. 64 (1990)2759

32 T. Ericson and W. Weise, Pions and Nuclei, p.67 Clarendon Press Oxford, 1988

Figure Captions

1. Diagrams with the $N^* \rightarrow N(\pi\pi)_{p-wave}$ decay.

2. Diagrams describing the reaction mechanisms that contribute to the pion induced pion production at $T_\pi = 280$ MeV. *a*) diagrams derived from the Weinberg Lagrangians, *b*) one Δ intermediate state diagrams, *c*) two Δ intermediate states diagrams, *d*) $N^*(\pi\pi)_{s_{wave}}$ diagrams, *e*) $N^*(\pi\pi)_{p-wave}$ diagrams.

3. Total cross section calculated with the pion pole term only (solid line), with the pion pole term and the $N^* \rightarrow N(\pi\pi)_{s-wave}$ diagrams (dashed line) and full calculation (dotted line).

4. Total cross section according to the model with C=-2.08 m_π^{-1}compared to experimental values of[3].

5. Calculated T_{π^+}(MeV) distributions (nb/sr^2MeV^2) and data for two geometrical configurations. 5a) Solid line: theoretical curves without Fermi motion. Dashed line: theoretical curves with Fermi motion included. 5b) Solid line: theoretical curves corrected for experimental conditions. Fermi motion not included. Dashed line: theoretical curves with Fermi motion included corrected for experimental conditions.

6. T_{π^+} theoretical distributions compared to data. QQD at 50°. $g_{N^*\Delta\pi} = 1.3m_\pi^{-1}$. Short-dashed curve: f_Δ=0.0; solid curve: f_Δ=0.1; dotted curve: f_Δ=0.5; long-dashed curve: f_Δ=1.0; dashed-dotted curve f_Δ=2.0. Kinetic energy of the incident pion is 280 MeV.

7. T_{π^+} theoretical distributions compared to data. QQD at 80°. $g_{N^*\Delta\pi} = 1.3m_\pi^{-1}$. Short-dashed curve: f_Δ=0.0; solid curve: f_Δ=0.1; dotted curve: f_Δ=0.5; long-dashed curve: f_Δ=1.0; dashed-dotted curve f_Δ=2.0. Kinetic energy of the incident pion is 280 MeV.

8. T_{π^-} and θ_{π^+} theoretical distributions compared to data. QQD at 50°. $g_{N^*\Delta\pi} = 1.3m_\pi^{-1}$. Short-dashed curve: f_Δ=0.0; solid curve: f_Δ=0.1; dotted curve: f_Δ=0.5; long-dashed curve: f_Δ=1.0; dashed-dotted curve f_Δ=2.0. Kinetic energy of the incident pion is 280 MeV.

9. T_{π^-} and θ_{π^+} theoretical distributions compared to data. QQD at 80°. $g_{N^*\Delta\pi} = 1.3m_\pi^{-1}$. Short-dashed curve: f_Δ=0.0; solid curve: f_Δ=0.1; dotted curve: f_Δ=0.5; long-dashed curve: f_Δ=1.0; dashed-dotted curve f_Δ=2.0. Kinetic energy of the incident pion is 280 MeV.

10. Reduced χ^2 value as a function of f_Δ variation. The three curves correspond to three different $g_{N^*\Delta\pi}$values. The lines connect the points.

Table Captions

1. Apparatus settings.

2. Total cross section sensitivity to the coupling constants variation. The coupling constant f_Δ is expressed in units ($4/5\ f_{NN\pi}$).

3. Calculated total cross section values for three sets of parameters. Errors are due to the statistical accuracy of the Monte Carlo approach of the theoretical model. First column:total cross section four experiment. Second column: total cross section for the free process at $T_\pi = 280$ MeV. Third column: total cross section for the quasifree process at $T_\pi = 256$ MeV. Bottom line: experimental values.

$\theta_{QQD}(°)$	$T_{QQD}(MeV)$	$\theta_{CARUZ}(°)$
80	50	-50
	80	-50
	50	-100
	80	-100
50	50	-50
	80	-50
	50	-100
	80	-100

T_π(MeV)	$\Delta\sigma(C = -1.52 \rightarrow -3.04)$ $g_{N^*\Delta\pi} = 1.5\ m_\pi^{-1}$ $f_\Delta = 1.$	$\Delta\sigma(g_{N^*\Delta\pi}$=1.08$\rightarrow$ 1.52) C = -2.0 m_π^{-1} $f_\Delta = 1.$	$\Delta\sigma(f_\Delta$=.5$\rightarrow$ 1.) C = -2.0 m_π^{-1} $g_{N^*\Delta\pi} = 1.5\ m_\pi^{-1}$
203	120 %	not detectable	not detectable
230	100 %	not detectable	not detectable
255	100 %	1 %	not detectable
280	100 %	5 %	4 %

C (m_π^{-1})	$g_{N^*\Delta\pi}$ (m_π^{-1})	f_Δ (m_π^{-1})	$\sigma_{t_{T_\pi=280MeV}}$ (μb)	$\sigma_{t_{T_\pi=280MeV}}$ (μb)	$\sigma_{t_{T_\pi=256MeV}}$ (μb)
			quasifree calc.	free calc.	quasifree calc.
-2.08	1.08	0.0	316 $\pm$ 4	319 $\pm$ 4	156 $\pm$ 2
-2.08	1.08	0.5	317 $\pm$ 4	319 $\pm$ 4	160 $\pm$ 3
-2.08	1.53	0.8	340 $\pm$ 4	336 $\pm$ 4	172 $\pm$ 3
				exp. value	exp. value
				384 $\pm$ 16^3	160 $\pm$ 10^{18}

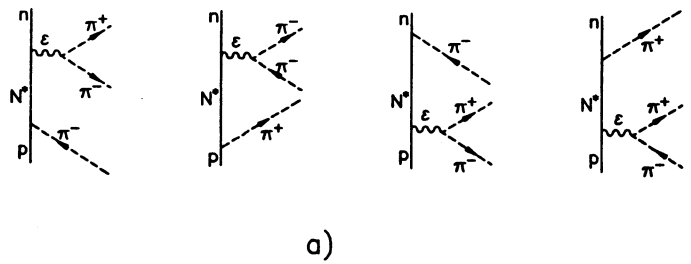

Fig. 1

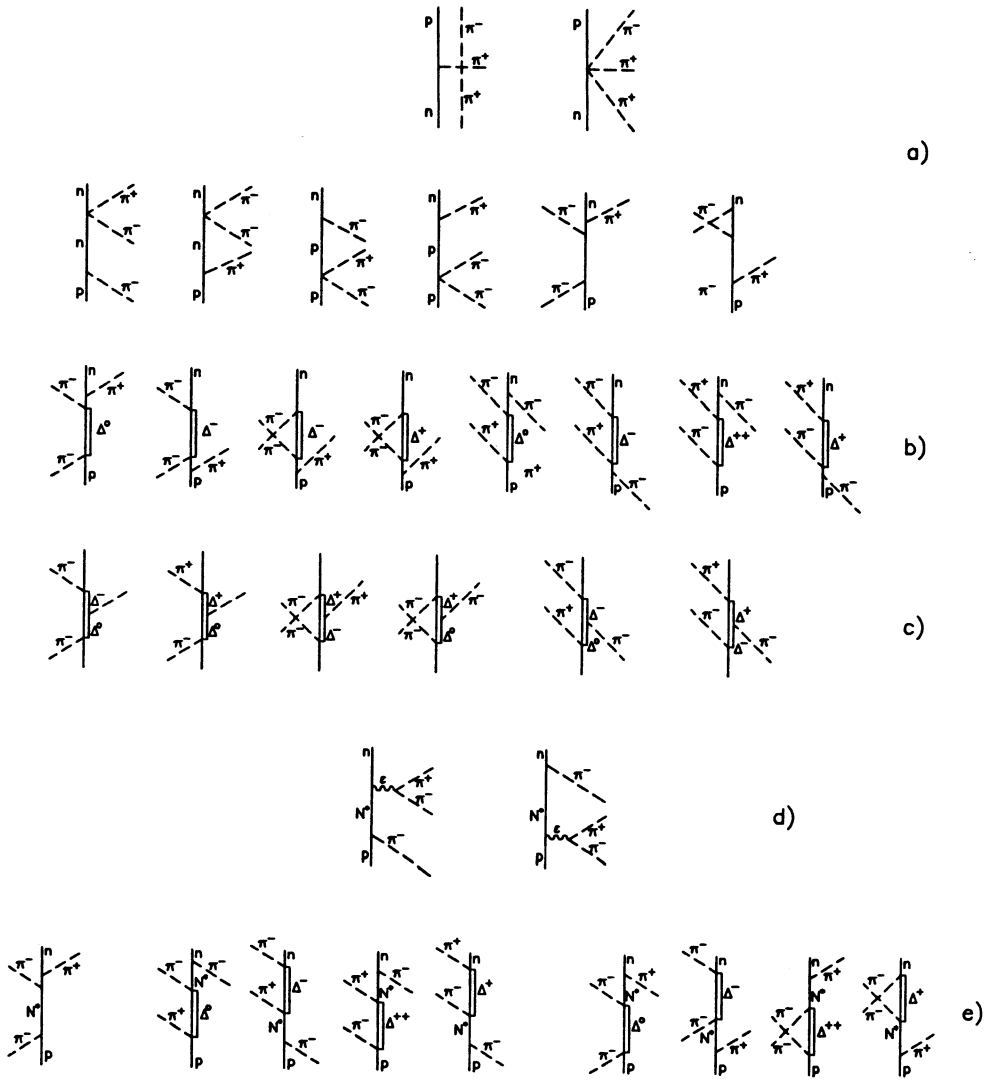

Fig. 2

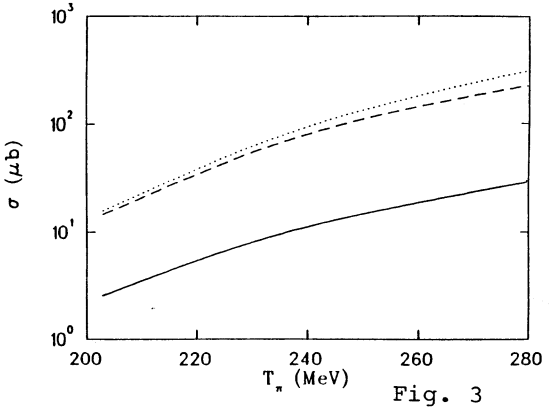

Fig. 3

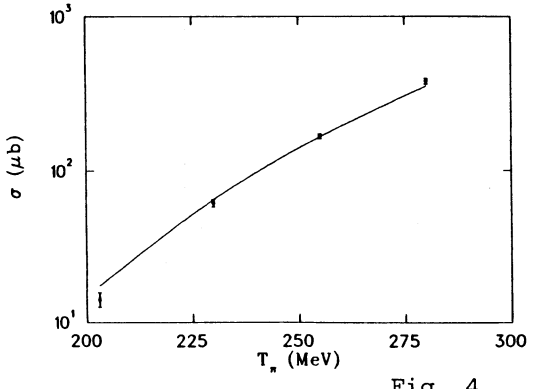

Fig. 4

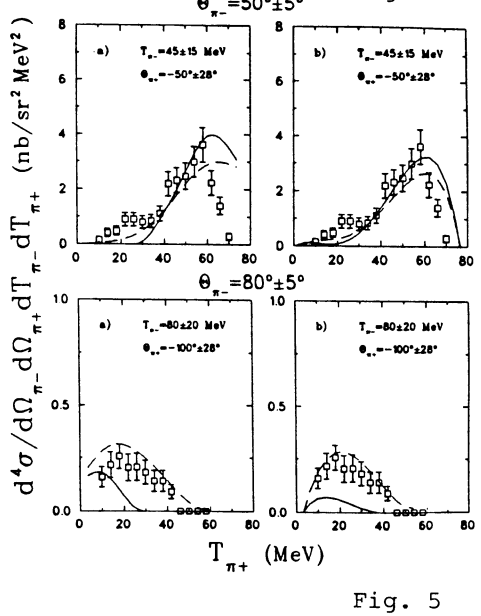

Fig. 5

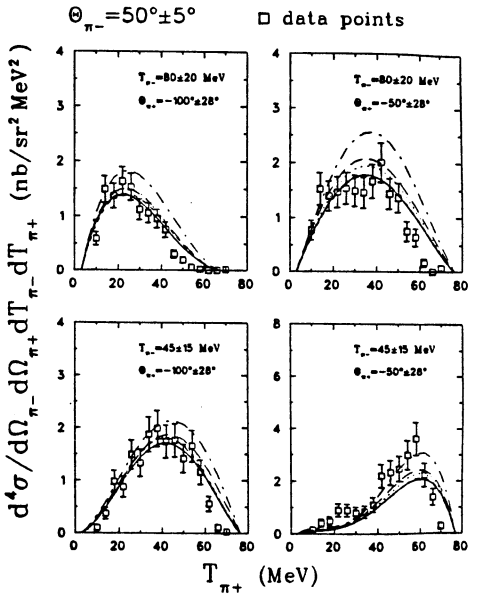

Fig. 6

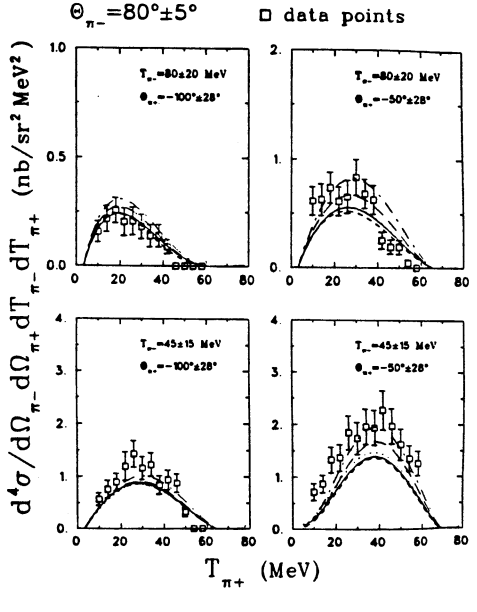

Fig. 7

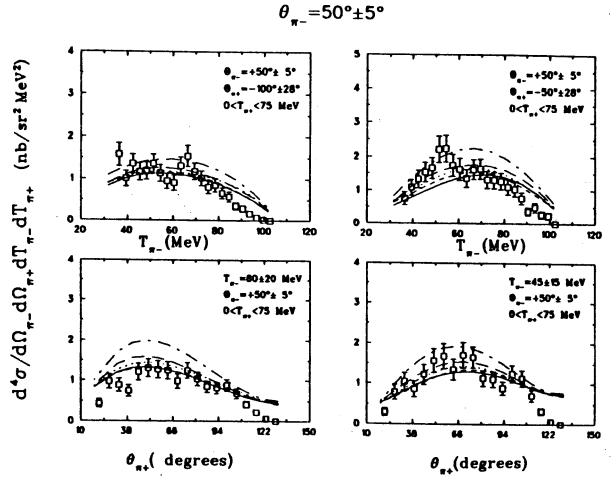

Fig. 8

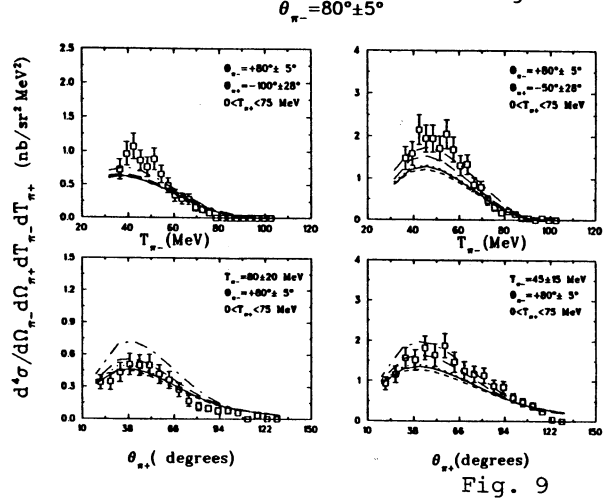

Fig. 9

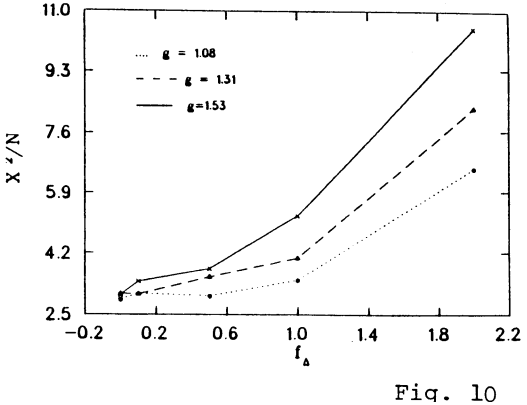

Fig. 10